Supplementary Information

Synthesis of Perfectly Ordered Mesoporous Carbons by Water-assisted Mechanochemical Self-assembly of Tannin

Jimena Castro-Gutiérrez,[a] Angela Sanchez-Sanchez,[a] Jaafar Ghanbaja,[a] Noel Díez,[b] Marta Sevilla,[b] Alain Celzard[a] and Vanessa Fierro[a]*

[a] Institute Jean Lamour, UMR CNRS, University of Lorraine, ENSTIB, 27 Rue Philippe Séguin, BP 21042, 88051 Epinal Cedex 9, France.

[b] Instituto Nacional del Carbón (CSIC), P.O. Box 73, Oviedo, 33080, Spain.

Table S1. Pore texture parameters, calculated from N_2 and CO_2 adsorption isotherms, of carbon materials: (i) prepared with various amounts of Pluronic® F127 and water, and used as references; (ii) obtained after various milling times; and (iii) synthesized with 2 g of aqueous HCl solutions with different pH values.

	Milling time [min]	S_{NLDFT} [m^2g^{-1}]	A_{BET} [m^2g^{-1}]	$V_{0.97,N_2}$ [cm^3g^{-1}]	$V_{\mu,NLDFT}$ [cm^3g^{-1}]	V_{meso} [cm^3g^{-1}]	F_{meso} [%]
(i) References							
CT2P0W0_60	60	829	578	0.25	0.23	0.02	8
CT2P0W2_60	60	503	231	0.10	0.11	--	--
CT2P2W0_60	60	672	466	0.36	0.17	0.19	53
(ii) Milling time							
CT2P2W2_30	30	735	543	0.46	0.18	0.28	60
CT2P2W2_45	45	683	497	0.46	0.16	0.30	64
CT2P2W2_60	60	695	522	0.47	0.16	0.30	65
CT2P2W2_75	75	703	521	0.44	0.17	0.27	61
CT2P2W2_90	90	709	538	0.46	0.18	0.28	61
CT2P2W2_120	120	663	484	0.40	0.16	0.24	60
(iii) pH							
CT2P2pH0_60	60	775	591	0.43	0.20	0.23	53
CT2P2pH1_60	60	713	533	0.51	0.17	0.34	67
CT2P2pH2_60	60	696	522	0.45	0.17	0.28	61
CT2P2pH3_60	60	713	528	0.44	0.18	0.26	60
CT2P2pH4_60	60	698	524	0.45	0.17	0.28	62

S_{NLDFT} and A_{BET}: specific surface areas calculated by applying NLDFT and BET models, respectively; $V_{0.97,N_2}$: total single point pore volume at relative pressure of 0.97; $V_{\mu,NLDFT}$: micropore volume from NLDFT model; $V_{meso} = V_{0.97,N_2} - V_{\mu,NLDFT}$: mesopore volume; $F_{meso} = V_{meso}/V_{0.97,N_2}$: mesopore fraction.

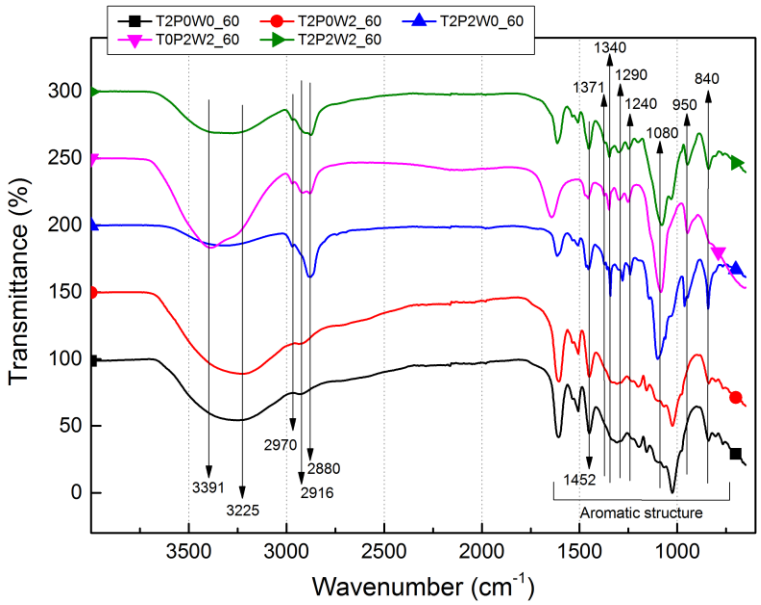

Figure S1. FTIR spectra of T2P2W2_60 and reference samples. The data were normalized with respect to a common peak (1452 cm^{-1}) and, for easier viewing, the spectra were shifted with respect to each other by 50% of transmittance.

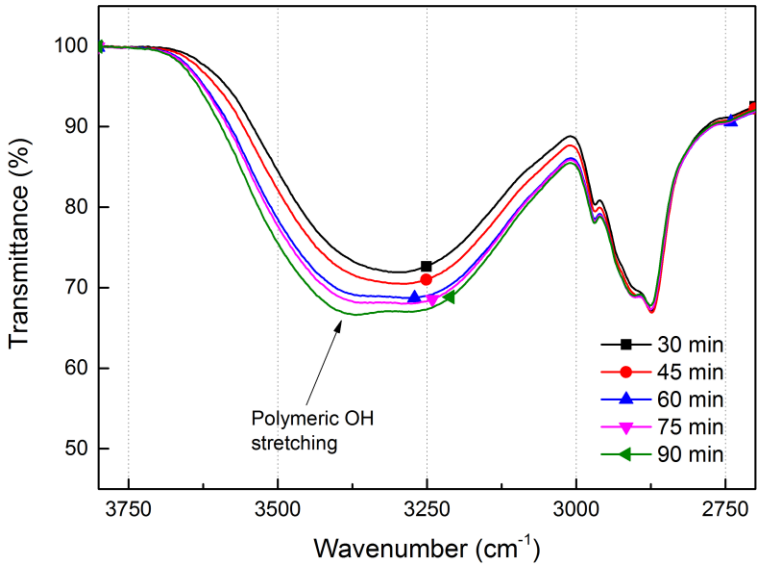

Figure S2. Detailed view of the FTIR spectra of samples T2P2W2_t synthesized during different milling times t, ranging from 30 to 90 min. For comparison, the data were normalized with respect to a common peak (1452 cm^{-1}).

Table S2. Peak assignment of FTIR spectra presented in Figure S1 and Figure S2.[1–3]

Aromatic structure of mimosa tannin	
Wavenumber [cm^{-1}]	Assignment
1606[a] ,1533, 1507	C=C stretching in pyrogallol-like B ring
1450[b]	C-C stretching in pyrogallol-like B ring
1200	C-O stretching of aromatic rings
1157[c]	Vibrations of resorcinol-like A ring
1025[c]	Overlapping stretching of C-O, C-C, C-OH, C-H bonds
766	Torsion of resorcinol-like A ring
Triblock copolymer Pluronic® F127	
Wavenumber [cm^{-1}]	Assignment
3391	Polymeric OH stretching
2970, 2916, 2880, 1371, 1340, 950, 840	C-H bonds
1290, 1240, 1080	C-O bonds

[a] Some authors assigned this peak to OH bending or C=O stretching,[1] explaining why a peak around 1640 cm^{-1} also appears in T0P2W2_60 spectrum.

[b] This peak appears also in T0P2W2_60 spectrum because of the C-C bonds; however, the intensity is lower in comparison with the samples containing tannin.

[c] Low-intensity peak. For samples containing P, this peak overlaps the strong peak at 1080 cm^{-1} due to the C-O bonds.

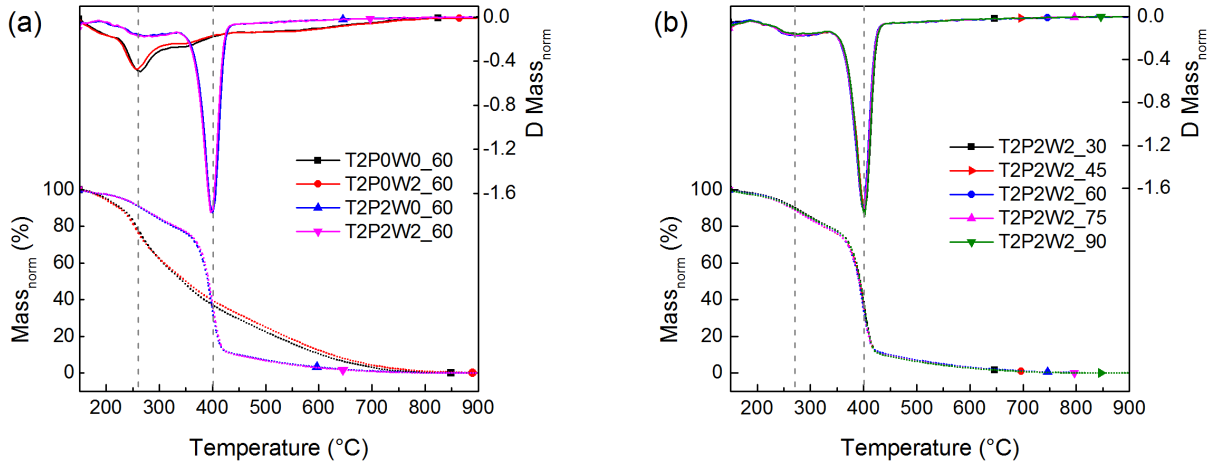

Figure S3. Absolute (left scale) and differential (right scale) normalized mass losses of: (a) T2P2W2_60 and reference samples; and (b) samples T2P2W2_t prepared at various milling times t, ranging from 30 to 90 min. The normalization was performed after removing the mass loss attributed to the evaporation of water.

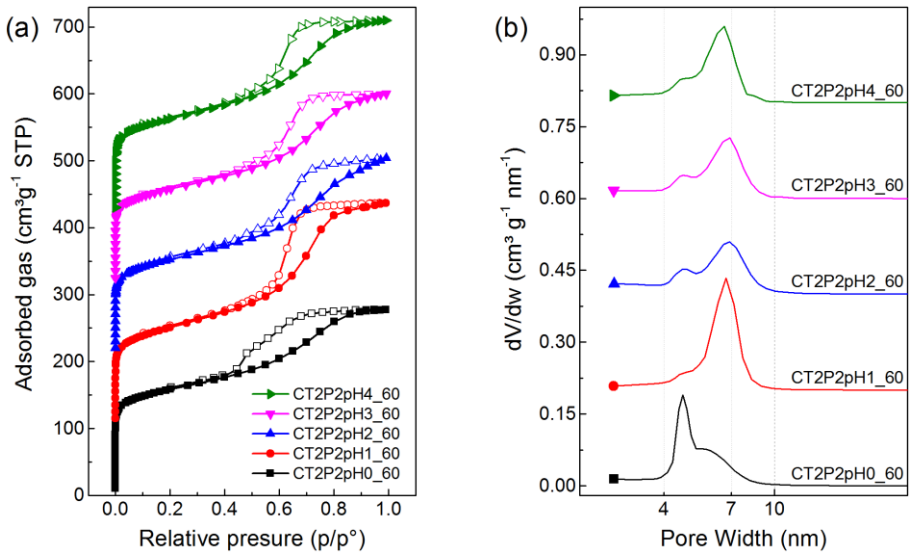

Figure S4. (a) N_2 adsorption-desorption isotherms and (b) corresponding PSDs of carbon materials CT2P2pHx_60, synthesized by using aqueous solutions of HCl at pH ranging from 0 to 4 instead of water, and a milling time of 60 min. For easier viewing, the curves were shifted with respect to each other by 105 cm^3 g^{-1} STP for isotherms and by 0.2 cm^3 g^{-1} nm^{-1} for PSDs.

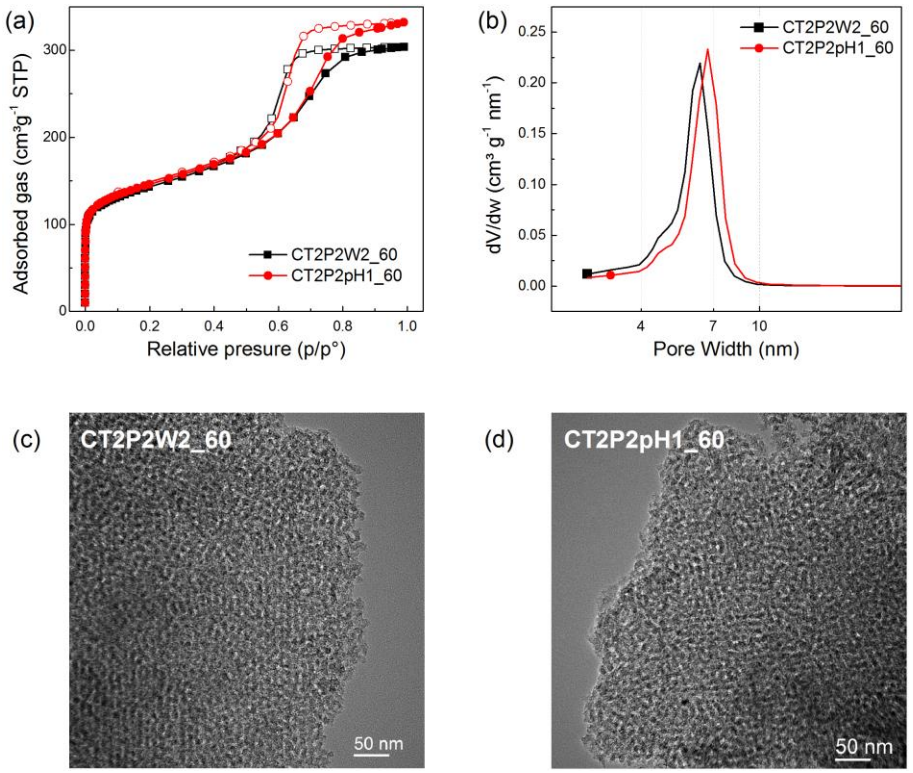

Figure S5. Comparison between CT2P2W2_60 and CT2P2pH1_60: (a) N_2 adsorption-desorption isotherms; (b) PSDs; and (c,d) TEM images.

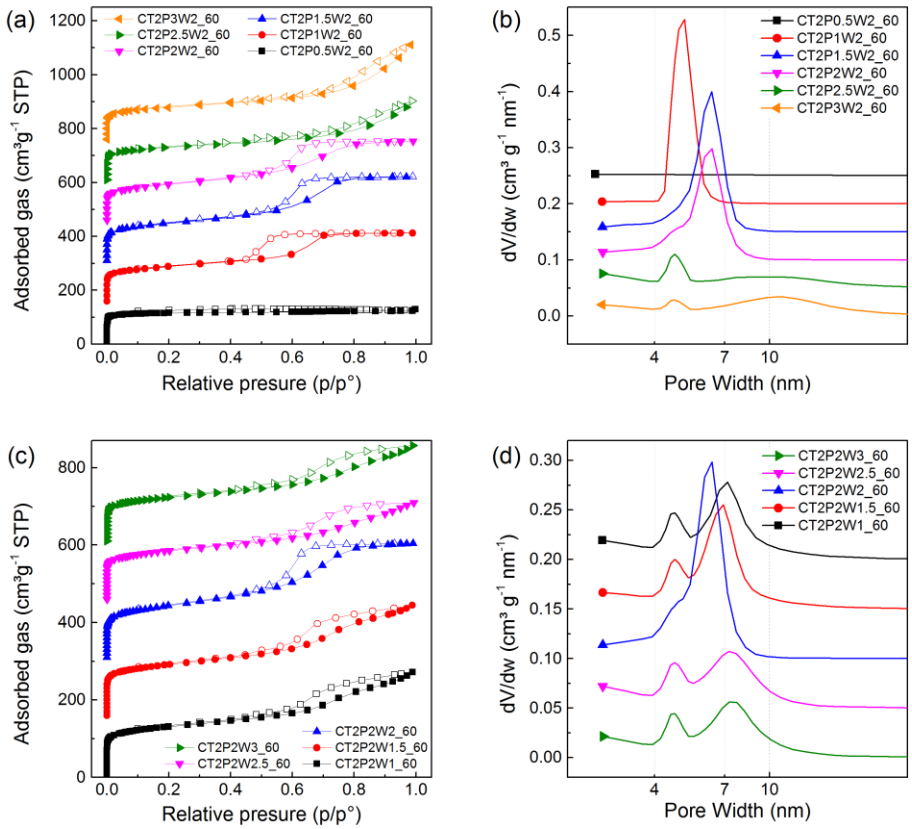

Figure S6. (a,c) N_2 adsorption-desorption isotherms and (b,d) corresponding PSDs of carbon materials synthesized using 60 min of milling and various P:W weight ratios. For easier viewing, the curves were shifted with respect to each other by 150 cm^3 g^{-1} STP for isotherms and by 0.05 cm^3 g^{-1} nm^{-1} for PSDs.

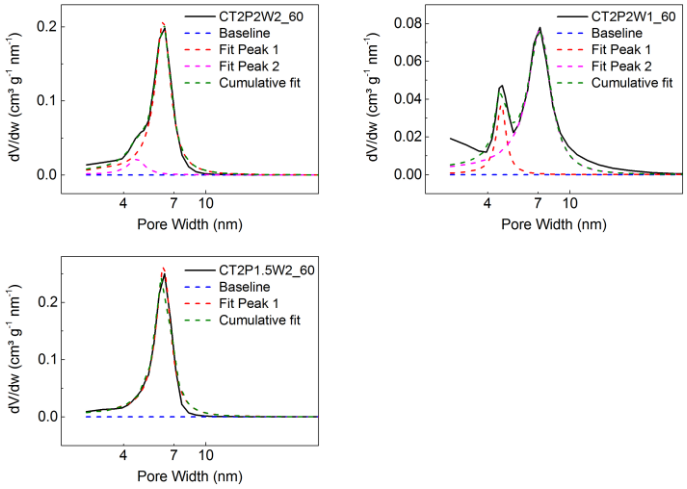

Figure S7. Examples of deconvolution into Lorentzian contributions performed on the PSDs of CT2P2W2_60, CT2P2W1_60 and CT2P1.5W2_60 samples.

Table S3. Characteristics of the main peaks in the PSDs of carbon materials synthesized using 60 min of milling and various P:W weight ratios.

	Maximum height (M) [$cm^3\ g^{-1}\ nm^{-1}$]	FWHM [nm]	M / FWHM	Peak position [nm]
CT2P0W2_60	0.0	--	0.0	--
CT20.5W2_60	0.0	--	0.0	--
CT2P1W2_60	0.37	0.73	0.50	5.0
CT2P1.5W2_60	0.26	1.24	0.21	6.2
CT2P2W2_60	0.02 0.23	1.13 1.20	0.02 0.19	4.7 6.2
CT2P2.5W2_60	0.05 0.02	0.51 17.22	0.10 0.001	4.7 10.3
CT2P3W2_60	0.02 0.03	0.48 10.65	0.03 0.003	4.7 11.3
CT2P2W0_60	0.03 0.03	0.44 7.40	0.06 0.004	4.7 7.0
CT2P2W1_60	0.04 0.08	0.61 2.21	0.06 0.03	4.7 7.1
CT2P2W1.5_60	0.04 0.11	0.59 1.84	0.06 0.06	4.7 6.8
CT2P2W2.5_60	0.03 0.06	0.63 3.42	0.05 0.02	4.7 7.4
CT2P2W3_60	0.03 0.06	0.58 3.37	0.06 0.02	4.6 7.6
CT2P0.5W1_60	0.0	--	0.0	--
CT2P0.5W1.5_60	0.09	0.71	0.12	4.1
CT2P0.75W1.25_60	0.25	0.54	0.46	4.4
CT2P0.75W1.5_60	0.44	0.37	1.20	4.5
CT2P0.75W1.75_60	0.56	0.32	1.77	4.6
CT2P1W1_60	0.31	0.87	0.35	4.7
CT2P1W1.25_60	0.34	0.82	0.42	5.0
CT2P1W1.5_60	0.47	0.60	0.78	4.9
CT2P1W1.75_60	0.31	0.94	0.33	5.2
CT2P1.25W1.25_60	0.29	0.99	0.29	5.9
CT2P1.25W1.5_60	0.25	1.21	0.21	6.0
CT2P1.25W1.75_60	0.23	1.26	0.18	5.9
CT2P1.5W1_60	0.27	1.21	0.22	6.2
CT2P1.5W1.25_60	0.25	1.35	0.18	6.1
CT2P1.5W1.5_60	0.31	1.04	0.30	6.2
CT2P1.5W1.75_60	0.30	1.11	0.27	6.1

Table S4. Pore texture parameters of samples synthesized with different P:W initial ratios and obtained after 60 min of ball-milling, calculated from N_2 and CO_2 isotherms.

	S_{NLDFT} (m^2g^{-1})	A_{BET} (m^2g^{-1})	$V_{0.97,N_2}$ (cm^3g^{-1})	$V_{\mu,NLDFT}$ (cm^3g^{-1})	V_{meso} (cm^3g^{-1})	F_{meso} (%)
CT2P0.5W1_60	566	304	0.12	0.13	--	--
CT2P0.5W1.5_60	732	529	0.25	0.20	0.05	18
CT2P0.5W2_60	657	457	0.19	0.18	0.01	3
CT2P0.75W1.25_60	659	477	0.30	0.17	0.12	41
CT2P0.75W1.5_60	731	537	0.35	0.19	0.15	44
CT2P0.75W1.75_60	761	567	0.36	0.20	0.16	44
CT2P1W1_60	733	546	0.42	0.18	0.24	57
CT2P1W1.25_60	755	568	0.44	0.19	0.25	57
CT2P1W1.5_60	750	556	0.44	0.19	0.25	58
CT2P1W1.75_60	784	587	0.47	0.19	0.28	59
CT2P1W2_60	712	508	0.41	0.17	0.24	58
CT2P1.25W1.25_60	713	532	0.46	0.17	0.29	63
CT2P1.25W1.5_60	732	547	0.49	0.17	0.31	64
CT2P1.25W1.75_60	696	527	0.45	0.17	0.28	62
CT2P1.5W1_60	742	565	0.51	0.18	0.34	66
CT2P1.5W1.25_60	715	539	0.49	0.17	0.32	66
CT2P1.5W1.5_60	767	588	0.52	0.18	0.34	65
CT2P1.5W1.75_60	750	577	0.53	0.18	0.35	66
CT2P1.5W2_60	726	541	0.50	0.17	0.33	66
CT2P2W1_60	689	486	0.40	0.17	0.23	58
CT2P2W1.5_60	721	524	0.44	0.18	0.26	60
CT2P2W2_60	695	522	0.47	0.16	0.30	65
CT2P2W2.5_60	696	503	0.39	0.18	0.21	54
CT2P2W3_60	641	454	0.38	0.16	0.22	59
CT2P2.5W2_60	686	486	0.43	0.17	0.26	60
CT2P3W2_60	638	476	0.53	0.16	0.37	70

S_{NLDFT} and A_{BET}: specific surface areas calculated by applying NLDFT and BET models, respectively; $V_{0.97,N_2}$: total single point pore volume at relative pressure of 0.97; $V_{\mu,NLDFT}$: micropore volume from NLDFT model; $V_{meso} = V_{0.97,N_2} - V_{\mu,NLDFT}$: mesopore volume; $F_{meso} = V_{meso}/V_{0.97,N_2}$: mesopore fraction.

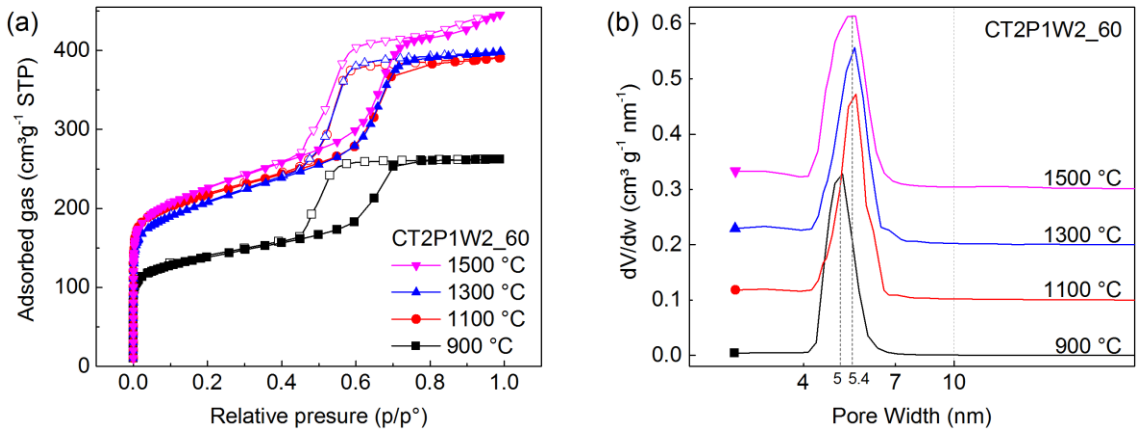

Figure S8. (a) N_2 adsorption-desorption isotherms and (b) corresponding PSDs for CT2P1W2_60 pyrolyzed at different temperatures. For easier viewing, the PSDs curves were shifted with respect to each other by 0.1 cm^3 g^{-1} nm^{-1}.

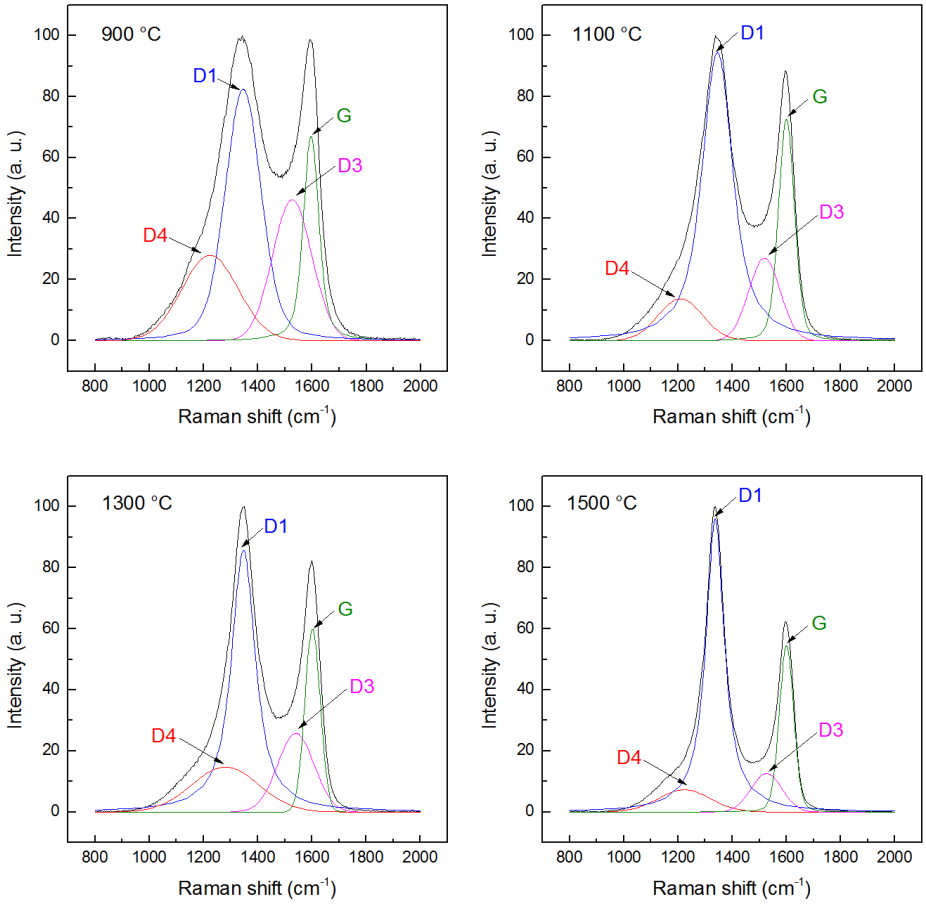

Figure S9. Raman spectra of CT2P1W2_60 pyrolyzed at different temperatures, and corresponding D_1, D_3, D_4 and G bands.

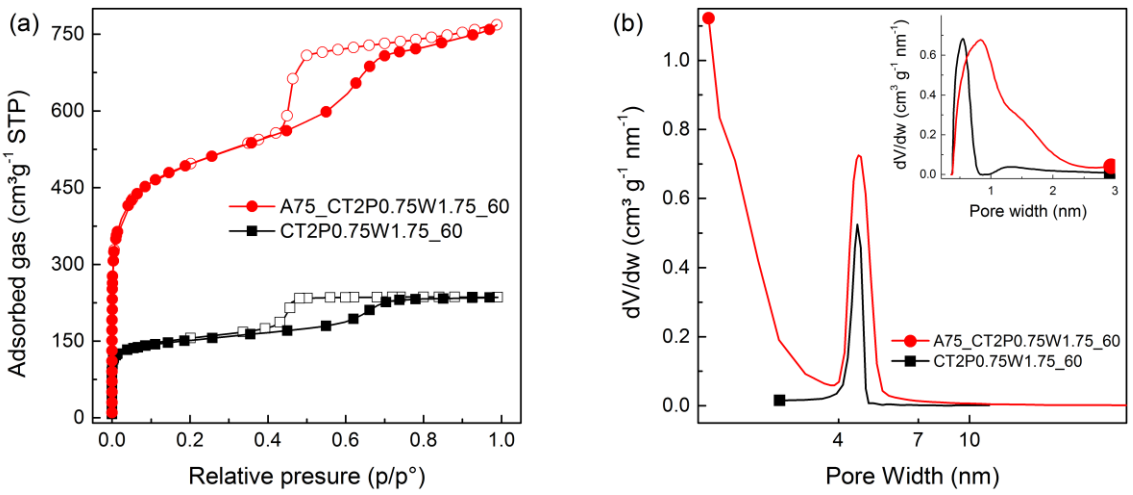

Figure S10. (a) N_2 adsorption-desorption isotherms, and (b) corresponding PSD for one OMC before (CT2P0.75W1.75_60) and after (A75_CT2P0.75W1.75_60) activation with CO_2 for 75 min at 900°C. The inset in (b) shows the DFT PSD in the micropore range for both materials.

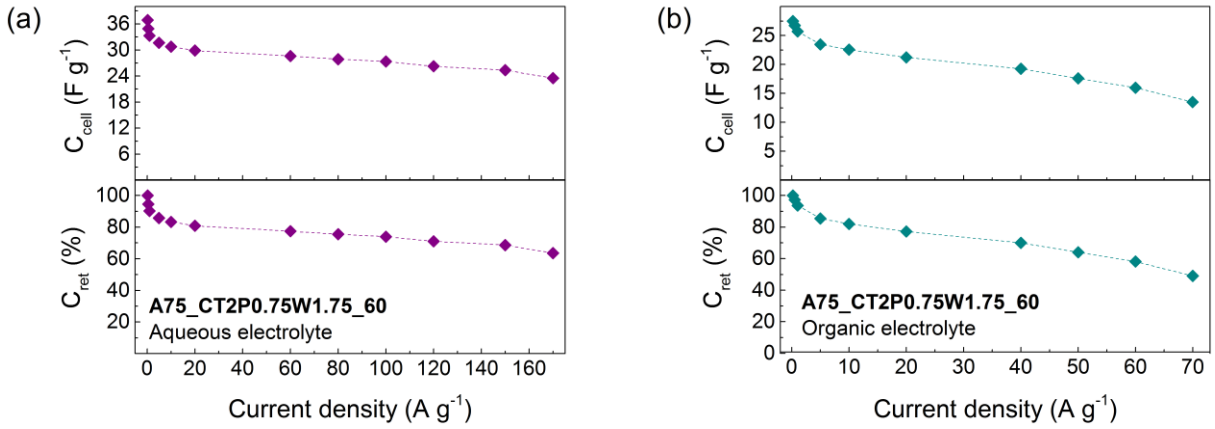

Figure S11. Evolution of cell capacitance (C_{cell}) and capacitance retention (C_{ret}) with current density for A75_CT2P0.75W1.75_60 in (a) aqueous and (b) organic electrolyte.

Table S5. Electrochemical performances of different carbon materials reported in the literature.

Carbon precursor/ Synthesis method	Carbon material	Electrolyte (cell voltage)	Capacitance [F g^{-1}]	Current density [A g^{-1}]	Energy density [Wh kg^{-1}]	Power density [kW kg^{-1}]	Ref. in ESI (Ref. in article)
Polyphenols: Phloroglucinol, gallic acid, catechin, and mimosa tannin/ Hard-templating (SBA-15); carbonization	OMCs: 2D-Hexagonal.	1 M H_2SO_4 (0.8 V)	~196 ~127	0.1 12	2.27 – 4.08 2.46 – 4.46 1.31 – 4.18 1.91 – 4.62	6.83 – 0.06 5.97 – 0.05 5.17 – 0.01 6.56 – 0.06	4 (62)
Sugarcane molasses/ HTC; carbonization	Oxygen rich carbons.	1 M H_2SO_4 (0.7 V)	32 13	0.1 1	~0.04 – ~1.8 ~0.35 – ~6.9 ~0.03 – ~0.6 ~0.45 – ~6.9	3 – ~0.15 ~5.5 – 0.5 ~4.5 – ~0.15 ~5 – ~0.13	5 (63)
Mesoporous SiC/ Si etching	Microporous nanorods	1 M H_2SO_4 (0.6 V)	~150 – ~190 ~130 – 150	0.1 15.5	-	-	6 (64)
Willow catkins/ Carbonization; KOH activation	Hollow fibrous structure.	6 M KOH (1 V)	333[a] 209[a]	0.1 10	5 – 8.8	5 – 0.05	7 (65)
Sucrose/ Hard-templating (MCM-48 and SBA-15); carbonization	OMCs: 3D cubic, 2D hexagonal rods and 2D hexagonal pipes.	30 wt.% KOH (0.9 V)	-	-	~4 – ~6 ~4.7 – ~5.4 ~5.4 – ~5.9	~0.8 – ~0.1 ~0.95 – ~0.1 ~1.05 – ~0.1	8 (66)
Seaweed/ Carbonization; KOH activation	Micro-mesoporous carbon with egg-box structure	1 M H_2SO_4 (1 V) 1M $TEABF_4$/AN (2.5 V)	425 280 210 156	0.1 100 0.1 50	- 25 – 42	- 29 – 0.39	9 (67)

Table S5 (Continued). Electrochemical performances of different carbon materials reported in the literature.

Carbon precursor/ Synthesis method	Carbon material	Electrolyte (cell voltage)	Capacitance [F g^{-1}]	Current density [A g^{-1}]	Energy density [Wh kg^{-1}]	Power density [kW kg^{-1}]	Ref. in ESI (Ref. in article)
Sodium gluconate/ Carbonization	Micro-mesoporous carbon nanosheets	1 M H_2SO_4 (1 V)	175 – 220 80 – 140	0.05 150	~1 – ~6 ~1.5 – ~6 ~3 – ~8	~20 – ~0.02 ~20 – ~0.02 ~30 – 0.02	10 (59)
		1M $TEABF_4$/AN (2.7 V)	100 – 135 50 – 100	0.05 120	~7 – 23 ~13 – ~33 16 – ~26	~90 – ~0.07 110 – ~0.07 110 – ~0.07	
Furfuryl alcohol/ Hard templating (Silica)	OMCs: 3D cubic; 3D low ordered. Worwhole-like pores.	1M $TEABF_4$/AN (2 V)	~95	~0.06	~3.5 – ~13	~5.7 – ~0.04	11 (68)
Peanut shell and rice husk/ $ZnCl_2$ activation	Disordered mesoporous carbons	1M $TEABF_4$/PC (2.7 V)	99 79	0.05 3	19.3 – 26.6	1.01– ~0.07	12 (69)
Resol and Pluronic/ Two-step template synthesis: latex spheres and silica hard template Thermosetting; carbonization; HF washing.	Ordered mesoporous carbon sphere arrays	1M $TEABF_4$/PC (3 V)	84	0.1	-	-	13 (70)

[a] Capacitance values calculated from galvanostatic charge-discharge in a three-electrode cell.

Calculation of electrochemical properties

The specific cell capacitances (C_{cell}, F g^{-1}) were calculated from CV data through Equation S1:

$$C_{cell} = \frac{\int I dV}{s\,\Delta V\,m} \quad (1)$$

where I is the current (A), s is the scan rate (V s^{-1}), ΔV is the potential window (V), and m is the mass of active material in the two electrodes (g).

GCD curves were used to calculate the specific capacitances of the cell (C_{cell}, F g^{-1}), the energy densities (E, Wh kg^{-1}) and the power densities (P, W kg^{-1}) by application of Equation S2, S3 and S4, respectively:

$$C_{cell} = \frac{I\,\Delta t}{m(\Delta V - iR)} \quad (2)$$

$$E = \frac{1}{2} C_{cell}(\Delta V - iR)^2 \quad (3)$$

$$P = \frac{E}{\Delta t} \quad (4)$$

where I is the discharge current (A); Δt is the discharge time (s), and iR is the potential drop due to inner resistance.

The single electrode specific capacitances, C_e, can be estimated by Equation S5:

$$C_e \approx 4\,C_{cell} \quad (5)$$

References

1 A. Ricci, K. J. Olejar, G. P. Parpinello, P. A. Kilmartin and A. Versari, *Applied Spectroscopy Reviews*, 2015, **50**, 407–442.
2 G. Tondi and A. Petutschnigg, *Industrial Crops and Products*, 2015, **65**, 422–428.
3 J. Coates, *Encyclopedia of analytical chemistry*.
4 A. Sanchez-Sanchez, M. T. Izquierdo, J. Ghanbaja, G. Medjahdi, S. Mathieu, A. Celzard and V. Fierro, *Journal of Power Sources*, 2017, **344**, 15–24.
5 A. Sanchez-Sanchez, A. Martinez de Yuso, F. L. Braghiroli, M. T. Izquierdo, E. D. Alvarez, E. Pérez-Cappe, Y. Mosqueda, V. Fierro and A. Celzard, *RSC Advances*, 2016, **6**, 88826–88836.
6 M. Rose, Y. Korenblit, E. Kockrick, L. Borchardt, M. Oschatz, S. Kaskel and G. Yushin, *Small*, 2011, **7**, 1108–1117.
7 K. Wang, Y. Song, R. Yan, N. Zhao, X. Tian, X. Li, Q. Guo and Z. Liu, *Applied Surface Science*, 2017, **394**, 569–577.
8 W. Xing, S. Z. Qiao, R. G. Ding, F. Li, G. Q. Lu, Z. F. Yan and H. M. Cheng, *Carbon*, 2006, **44**, 216–224.
9 D. Kang, Q. Liu, J. Gu, Y. Su, W. Zhang and D. Zhang, *ACS Nano*, 2015, **9**, 11225–11233.
10 A. B. Fuertes and M. Sevilla, *ACS Applied Materials & Interfaces*, 2015, **7**, 4344–4353.
11 M. Sevilla, S. Álvarez, T. A. Centeno, A. B. Fuertes and F. Stoeckli, *Electrochimica Acta*, 2007, **52**, 3207–3215.
12 X. He, P. Ling, J. Qiu, M. Yu, X. Zhang, C. Yu and M. Zheng, *Journal of Power Sources*, 2013, **240**, 109–113.
13 H.-J. Liu, W.-J. Cui, L.-H. Jin, C.-X. Wang and Y.-Y. Xia, *Journal of Materials Chemistry*, 2009, **19**, 3661.